Analysis of Drone Placement Strategies for Complete Interference Cancellation in Two-Cell NOMA CoMP Systems

Antoine Kilzi, Joumana Farah, Charbel Abdel Nour, Catherine Douillard

IEEE Access
Multidisciplinary | Rapid Review | Open Access Journal

Received September 16, 2020, accepted September 25, 2020, date of publication September 29, 2020,
date of current version October 9, 2020.

Digital Object Identifier 10.1109/ACCESS.2020.3027538

Analysis of Drone Placement Strategies for Complete Interference Cancellation in Two-Cell NOMA CoMP Systems

ANTOINE KILZI[1], (Student Member, IEEE), JOUMANA FARAH[2], (Member, IEEE), CHARBEL ABDEL NOUR[1], (Senior Member, IEEE), AND CATHERINE DOUILLARD[1], (Senior Member, IEEE)

[1]IMT Atlantique, Lab-STICC, UMR CNRS 6285, F-29238 Brest, France
[2]Department of Electricity and Electronics, Faculty of Engineering, Lebanese University, Beirut 27622819, Lebanon

Corresponding author: Antoine Kilzi (antoine.kilzi@imt-atlantique.fr)

This work was supported in part by Institut Mines-Télécom (IMT) Atlantique, and in part by the Lebanese University Research Support Program.

ABSTRACT The use of unmanned aerial vehicles (UAV) as flying base stations is rapidly growing in the field of wireless communications to leverage the capacity of congested cells. This study considers a two-cell system where one of the cells is saturated, i.e. can no longer serve its users, and is supported by a UAV. The UAV positioning problem is investigated specifically to benefit from the interference cancellation properties available through the introduction of power-domain non-orthogonal multiple access (NOMA) techniques in coordinated multipoint (CoMP) systems. Indeed, adequate placement of the UAV can enable triple mutual successive interference cancellation (TMSIC) between a triplet of users, including a cell-edge and a cell-center user in each cell, to maximize system throughput or a mixture of throughput and TMSIC probability. The random line-of-sight/non-line-of-sight realizations of air-to-ground links between users and UAV are taken into account in the problem modeling, showing a significant improvement in performance compared to the conventional mean path loss model. The performance evaluation highlights the existing trade-offs between system capacity, fairness, and computational complexity of the investigated approaches.

INDEX TERMS Unmanned aerial vehicle, coordinated multipoint, non-orthogonal multiple access, successive interference cancellation, triple mutual successive interference cancellation.

I. INTRODUCTION

Unmanned aerial vehicles (UAV) have lately been gathering interest as a growing research topic for mobile communication networks [1]–[5]. The major capabilities of UAVs reside in their fast and cost-effective setup and their virtually unconstrained mobility in the aerial space, largely improving the probability of line-of-sight (LoS) communication. Unlike terrestrial mobile base stations that are bound by road maps and traffic light constraints for circulation, UAVs can move freely through space to cope with the evolving demand for service or network reconfiguration. Many applications require such key capabilities, ranging from natural disaster scenarios like floods, hurricanes and tornadoes, to public safety communication, and temporary crowded events like concerts or festivals in large arenas, sports events in football stadiums, etc. While deploying additional small base stations (BSs) in anticipation to planned events such as festivals could be profitable for the case of long lasting events (expanding over a few days), it is not suited for dealing with temporary and unpredictable emergency situations typically spanning over the course of a couple of minutes to a few hours. Such scenarios could be rooted to exceptional events like for the cases of disaster relief and service recovery, as well as to much more common congestion scenarios like antenna failure or energy shortage, actual traffic jamming resulting in uneven data traffic loads, etc. Deploying additional small cells especially for that matter equates to large expenditure costs for small periods of time, hence the inefficiency of such approaches. Relying on UAVs for these systems is an appealing feature thanks to their on-demand service capabilities (they can be released and retrieved after use), their adjustable position in real time which can cope with high data traffic variation, and their cost-effective and fast deployment. Therefore, the use

The associate editor coordinating the review of this manuscript and approving it for publication was Xiaofei Wang.

of UAVs in the system provides greater flexibility and better preparedness to respond to all sorts of wireless demands occurring in a rather difficult-to-predict manner [6].

Lately, non-orthogonal multiple access (NOMA) has received much attention in both academia and industry for its capabilities to efficiently increase system capacity and accommodate more user-equipments (UE) than orthogonal multiple access (OMA) techniques [7]–[14]. This is done by superposing the signals of two or more users in both time and frequency domains at transmission, and separating the signals at reception in the power domain. In downlink, the message with the largest power is decoded first and then subtracted from the total received signal, then the second largest power message is decoded and subtracted and so on. This successive interference cancellation (SIC) is done iteratively until the UE decodes its own message. Many works have tackled the integration of NOMA in UAV-assisted networks. The authors in [15] study the case of a UAV BS serving a large number of users using NOMA. A simultaneous optimization of the UAV height, the bandwidth allocation to users, the transmit antenna beamwidth and power allocation (PA) is conducted to solve the max-min rate problem using inner convex approximations. The results show that NOMA outperforms OMA in this context, achieving results close to dirty paper coding. However, the UAV's horizontal position is fixed at the center of the cell and the user pairing strategy is based on the Euclidean distance between a far-user and a nearby-user. In contrast, the work in [16] proposes a heuristic pairing strategy for multi-user systems inspired by the optimal PA and UAV placement solution for rate maximization of a single NOMA pair. Bisection search is used afterwards to determine the optimal PA and UAV placement for the maximization of the minimum sum rate of user pairs. A UAV-assisted NOMA network is proposed in [17] where a fixed BS and a UAV cooperate to serve users. The sum rate maximization is accomplished by optimizing the rate of UAV-served users through trajectory and scheduling optimization first, then NOMA precoding is optimized to maximize BS-served user rates. In [18], a UAV is dispatched to upload specific information to ground BSs that serve uplink users with rate constraints. The objective for the UAV fly path is to complete its mission in the fastest possible time. To that end, a *fly-hover-fly* procedure is proposed, coupled with successive convex approximation (SCA) and uplink NOMA serving is used. The results show that mission completion time is significantly minimized with the proposed NOMA scheme compared to OMA.

The work in [19] focused on studying the performance of the UAV downlink command and control (C&C) channel, for which the 3GPP has defined minimum rate requirements. The study compared the deployment of a UAV for two network architectures: a traditional three-sector BS operating in OMA, and a massive MIMO cellular system operating in multi-user mode (i.e. multiple users scheduled per time-frequency resource). The use of MIMO with UAV improved reliability compared to traditional cells when supporting the data rate requirements of a C&C channel, thus allowing for higher altitude placement of UAVs compared to traditional cells. However, the study also revealed that UAVs can severely degrade the performance achieved by ground user equipments (GUEs) in MIMO if an uplink power control policy is not applied to protect the GUEs, which stresses the need for coordination between the aerial and ground networks.

Indeed, the integration of UAVs as aerial base stations supporting the ground network will require a better management of the system resources in time and frequency, since the backhaul link between the UAV and the network needs to be established and the hand-off procedures as well as low-latency control need to be guaranteed. Coordinated multi-point (CoMP) systems [20], [21] provide such a framework of cooperation between adjacent cells. In CoMP, cells can share the channel state information (CSI) of users to perform joint scheduling known as coordinated scheduling (CS-CoMP) and coordinated beamforming (CB-CoMP). When the user data information is shared between adjacent transmission points (TPs), more elaborate CoMP techniques such as dynamic point selection (DPS) and joint transmission (JT-CoMP) can be employed. In this study, we consider JT-CoMP where signals are transmitted to each user from multiple TPs.

In a previous work, we studied the combination of NOMA with CoMP for a two-cell system [22]. A full JT system over NOMA clusters of two and three users was studied showing significant advantages over partial JT (where JT is only used for cell-edge users and DPS is used for cell-center users). Sending the NOMA signals from different TPs enabled mutual SIC between users, i.e. all users canceling the signals of each other at the same time. This led to defining the conditions of dual mutual SIC (DMSIC) and triple mutual SIC (TMSIC) for two or three-user clusters respectively. The obtained interference-free NOMA clusters provided significantly better performance results than classical NOMA schemes in terms of spectral efficiency (SE) as well as fairness among users, which suggests positioning the UAV with the aim of favoring TMSIC application. Thus, coupling the interference cancellation capabilities of NOMA with CoMP and the mobility of UAVs aims for an effective inter-cell interference (ICI) cancellation. This ICI cancellation is all the more possible thanks to the management of the UAV mobility and power levels. Indeed, compared to fixed ground base stations (BSs), the UAV allows for both a reduction in the needed transmit power (by ensuring higher link qualities than conventional ground-to-BS channels) as well as a localization of the interference to the region the UAV is hovering over while serving users.

In this work, UAV positioning procedures are proposed to best alleviate the load on the congested cell. A particular attention is directed at enhancing system SE through a fairer serving of cell-edge users as well as cell-centered users of the two adjacent cells. The idea is to position the UAV such that the TMSIC conditions are satisfied, thus optimizing both throughput and fairness. The contributions of the paper can be summarized as follows:

- We study the UAV positioning problem while taking into account the specificity of LoS/non-LoS (NLoS) propagation between users and the UAV, instead of the mean path loss model.
- We introduce a probabilistic framework that enables the calculation of the TMSIC probability associated to the UAV position. This enables the formulation of a UAV positioning problem to maximize the chances of TMSIC between users.
- We investigate several positioning techniques based on the probabilistic framework with different optimization criteria, and we compare them to positioning techniques based on traditional mean path loss consideration, in terms of achieved throughput and fairness.

This paper is organized as follows: section II describes the system model and formulates the general UAV placement problem. Section III introduces the mathematical framework for modeling the UAV positioning problem on a probabilistic basis. In section IV, the proposed UAV positioning techniques are presented, while power allocation strategies are defined in section V. In section VI, the performance results are assessed, and section VII draws the major conclusions of this study.

II. SYSTEM MODEL

A two-cell system is considered where each cell is originally served by a unique BS located at its center. However, cell 2 is congested in a way that its BS can no longer serve additional users. A UAV is deployed to assist the congested system as shown in Fig. 1. The UAV may be controlled by an external controller or the BS of cell 1 itself which communicates to the UAV its flight path information and power allocation through a backhaul link. The management of the backhaul link to the BS is not considered in this paper and was studied in [23]. In such scenarios, UAV placement generally tends to favor the cell-edge users [24] that suffer from poor channel gains as well as significant potential interference due to the neighboring cell. However, while focusing exclusively on such users tends to boost the inter-user fairness within the cell, system throughput is not optimized and only marginal enhancements would occur on the throughput performance. To strike a balance between fairness and system throughput, cell-edge as well as cell-center users must be considered for the UAV placement problem. Moreover, to take advantage of the cooperation between the cells and to properly manage inter-cell interference, cell-center users from cell 1 and 2 should be considered as well. The interference management can be done through NOMA pairing of users from both cells, as was done in [22]. For this purpose, we focus our study on a three-user NOMA cluster formed by a triplet of users selected from regions 1, 2 and 3 of the two cells, as shown in Fig. 1, where each user can be representative of a user agglomeration from its respective region.

The fixed BS a_1 serves the users and is assisted by a UAV working as a mobile base station (MBS). The BS and MBS are both equipped with a single transmit antenna. It is assumed that the information to be transmitted for each user is made available at the level of the BS and MBS through the backhaul link, enabling DPS and JT serving in the system. JT-mode is used in the remainder of the study, given its superior performance to DPS, as shown in [22].

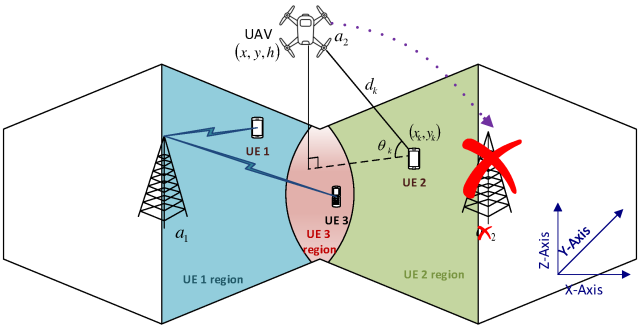

FIGURE 1. Illustration of the two-cell JT system with the functional base station a_1, the saturated BS in cell 2, the UAV working as MBS a_2, and the three colored user regions.

The objective of this study is to serve the three users such that the resulting channel gains from the UAV position allow the application of TMSIC on their sub-band. By doing so, system throughput and fairness would be optimized, as shown in [22]. Note that other users in the system are assumed to be served on different sub-bands, without causing interference on the considered user triplet. However, the UAV positioning only involves the user triplet that includes the cell-edge user. Additionally, it should be noted that despite Fig. 1 depicting a centralized antenna system (CAS), the proposed problem formulation provided next is applicable to distributed network architectures (distributed antenna systems, small cells, etc.), in which a_1 and a_2 of Fig. 1 play the role of two nearby antennas of adjacent cells.

In the following, the path loss model is presented, followed by the TMSIC conditions, then the TMSIC solution space is discussed. Afterwards, the UAV placement problem is formulated.

A. PATH LOSS MODEL

The air-to-ground (A2G) links between users and the UAV are either LoS or NLoS with some probability. Assuming that the UAV is located at position (x, y, h), and that user k is located at position (x_k, y_k) in the ground plane, the path loss for the LoS and NLoS links in dB is given respectively by [25]:

$$L_{\text{LoS}} = 20\log\left(\frac{4\pi f_c d_k}{c}\right) + \eta_{\text{LoS}}, \tag{1}$$

$$L_{\text{NLoS}} = 20\log\left(\frac{4\pi f_c d_k}{c}\right) + \eta_{\text{NLoS}}, \tag{2}$$

where c is the speed of light in vacuum, f_c is the carrier frequency, d_k is the distance between the UAV and user k (cf. Fig.1), η_{LoS} and η_{NLoS} are the average additional losses for LoS and NLoS transmissions. The probability of having a LoS link, P_{LoS}, depends on the angle θ_k formed by the UAV-user k segment and its projection on the ground plane:

$\theta_k = \tan^{-1}(h/\sqrt{(x-x_k)^2+(y-y_k)^2})$. P_{LoS} is modeled by:

$$P_{\text{LoS}} = \frac{1}{1+\alpha e^{-\beta\left(\frac{180}{\pi}\theta_k - \alpha\right)}}, \tag{3}$$

where α and β are constants that depend on the environment (suburban, urban, dense-urban, etc.) parameters [25], [26] such as the ratio of built-up land area to total land area, the number of buildings per unit area, and a scale parameter describing the building's heights distribution. Let $h_{k,i}$ be the squared channel gain between user k and BS a_i. The squared channel gain $h_{k,2}$ between the UAV and user k can be obtained from the experienced path loss L by:

$$h_{k,2} = 10^{-L/10} = \frac{c^2}{(4\pi f_c d_k)^2} \times \begin{cases} 10^{-\eta_{\text{LoS}}} & \text{for } L = L_{\text{LoS}}, \\ 10^{-\eta_{\text{NLoS}}} & \text{for } L = L_{\text{NLoS}}, \end{cases} \tag{4}$$

$h_{k,2}$ is then a function of the UAV position as well as the random channel realization regarding the LoS/NLoS nature of the user-UAV link.

B. SIGNAL MODEL AND TMSIC CONDITIONS

An adequate UAV placement is one that delivers channel links such that TMSIC is rendered feasible in that position. To enable TMSIC, a set of constraints must be satisfied including power multiplexing constraints (PMC) and rate constraints.

Let m, n and p denote the three users with s_m, s_n, and s_p their transmitted signals. Let $P_{p,r}$ be the power of the message s_p transmitted from antenna a_r to user p; reaching it with a power $P_{p,r}h_{p,r}$. Since both a_1 and a_2 are used for the transmission of the message to p, the received signal power is the sum of the received powers from both antennas, i.e. $P_{p,1}h_{p,1} + P_{p,2}h_{p,2}$. The rate or mutual SIC conditions between n and p define the conditions enabling mutual SIC between the two users from the information theory perspective [27]. They are given by:

$$\begin{cases} SINR_p^{s_n} > SINR_n^{s_n} & \text{SIC of } s_n \text{ at user } p, \quad (5) \\ SINR_n^{s_p} > SINR_p^{s_p} & \text{SIC of } s_p \text{ at user } n, \quad (6) \end{cases}$$

where $SINR_i^{s_j}$ is the signal-to-interference-plus-noise ratio (SINR) of s_j at the level of i. It is given by:

$$SINR_i^{s_j} = \frac{P_{j,1}h_{i,1} + P_{j,2}h_{i,2}}{\sum\limits_{u \in \mathcal{I}_i^{s_j}} (P_{u,1}h_{i,1} + P_{u,2}h_{i,2}) + N_0 B},$$

where B is the sub-band bandwidth, N_0 is the power spectral density of additive white Gaussian noise and with $\mathcal{I}_i^{s_j}$ the set of interfering users on i when decoding s_j. Achieving TMSIC resides in achieving mutual SIC between the three pairs (n, p), (p, m) and (m, n). Two decoding orders are possible at the level of each of the three users (e.g. for user m, decoding s_n then s_p or s_p then s_n), leading to eight combinations of possible decoding orders in the system. The impact of the decoding order is captured in the interfering sets such as $\mathcal{I}_p^{s_n}$. These sets are partitioned into a common interfering set $\mathcal{C}_{pn}^{s_n}$ and user-specific interfering sets $\mathcal{U}_n$ and $\mathcal{U}_p$ which are disjoint. Then, we have $\mathcal{I}_p^{s_n} = \mathcal{C}_{pn}^{s_n} \cup \mathcal{U}_p$, $\mathcal{I}_n^{s_n} = \mathcal{C}_{pn}^{s_n} \cup \mathcal{U}_n$. Condition (5) is rearranged in the appendix to lead to:

$$\begin{aligned} &h_{n,1}h_{p,1}P_{n,1} \\ &\Big[\sum_{i\in\mathcal{U}_n} P_{i,1} - \sum_{i\in\mathcal{U}_p} P_{i,1}\Big] + h_{p,2}h_{n,1}\Big[P_{n,2}\sum_{i\in\mathcal{U}_n} P_{i,1} - P_{n,1}\sum_{i\in\mathcal{U}_p} P_{i,2}\Big] \\ &+h_{n,2}h_{p,2}P_{n,2}\Big[\sum_{i\in\mathcal{U}_n} P_{i,2} - \sum_{i\in\mathcal{U}_p} P_{i,2}\Big] \\ &+h_{p,1}h_{n,2}\Big[P_{n,1}\sum_{i\in\mathcal{U}_n} P_{i,2} - P_{n,2}\sum_{i\in\mathcal{U}_p} P_{i,1}\Big] \\ &+(h_{p,1}h_{n,2} - h_{p,2}h_{n,1})\Big[P_{n,1}\sum_{i\in\mathcal{C}_{pn}^{s_n}} P_{i,2} - P_{n,2}\sum_{i\in\mathcal{C}_{pn}^{s_n}} P_{i,1}\Big] > 0 \end{aligned} \tag{7}$$

For a particular decoding order u, six similar rate constraints (two at the level of each user) must be verified to enable TMSIC, hence the corresponding set of SIC constraints $\mathcal{SIC}(u)$ accounting for the decoding order u. However, recall from (4) that $h_{k,2}$ depends on the LoS/NLoS realization of the A2G channel of user k. Thus, even for the same decoding order u, the SIC constraints change according to the LoS/NLoS A2G state of the three users in the cluster. These eight possible LoS/NLoS configurations among the users, coupled with the eight potential decoding orders, lead to a total of 64 possible combinations of decoding orders/random channel realizations. The SIC constraints are then denoted by $\mathcal{SIC}(i, u)$ for the i^{th} LoS/NLoS combination and u^{th} decoding order.

The PMCs on the other hand stipulate that if a signal s_p is to be decoded prior to other signals s_n, s_m at the level of a given user (users m or n), the power level of s_p must be greater than the power level of the combined signals s_n and s_m. This guarantees SIC stability, since every signal is ensured to be the dominant signal during its decoding [28], [29]. Since in TMSIC every user decodes the signal of the two other ones before retrieving its signal, six PMC constraints must be verified (for any LoS/NLoS combination i and any decoding order u), constituting a set denoted by $\mathcal{PMC}(i, u)$. For example, if in the selected decoding order p decodes n than m, the two corresponding PMCs are given by:

$$\begin{aligned} &P_{n,1}h_{p,1} + P_{n,2}h_{p,2} > (P_{m,1} + P_{p,1})h_{p,1} + (P_{m,2} + P_{p,2})h_{p,2} \\ &P_{m,1}h_{p,1} + P_{m,2}h_{p,2} > P_{p,1}h_{p,1} + P_{p,2}h_{p,2}. \end{aligned} \tag{8}$$

For more details, the reader is referred to [22]. The achieved rate by each user k, when JT-CoMP is used to apply TMSIC between the user triplet, is given by:

$$R_k = B\log_2\left(1 + \frac{\sum_{i=1}^{2} P_{k,i}h_{k,i}}{N_0 B}\right), \tag{9}$$

A final set of constraints is to account for the transmit power limits of a_1 and a_2 referred to as P_{L_1} and P_{L_2}:

$$P_{1,1} + P_{2,1} + P_{3,1} \leq P_{L_1},$$

$$P_{1,2} + P_{2,2} + P_{3,2} \leq P_{L_2}. \tag{10}$$

The first inequality accounts for the sum of the users powers over the antenna a_1, and the second one accounts for the sum power over antenna a_2. The problem then resides in finding the positions of the UAV such that: 1) the PMCs, 2) the mutual SIC constraints, and 3) the total transmit power constraints are satisfied.

C. TMSIC SOLUTION SPACE

When TMSIC feasibility is targeted, the problem at hand can be seen as one that admits several constraints with no objective function, and is therefore a constraint satisfaction problem (CSP). In other words, one would seek the set of UAV positions where TMSIC is feasible while respecting the constraints. We denote by $r_{i,n}$ the region of space in which the UAV can be placed such that TMSIC is possible, for the n^{th} decoding order, and the i^{th} LoS/NLoS configuration. If we let $\mathbb{D}$ be the allowed space region for UAV positioning, then the CSP for a combination (i, n) can be cast as:

$$\mathcal{CSP}_{i,n} : r_{i,n} = \{\boldsymbol{pos} \in \mathbb{D} / \mathcal{PMC}(i,n), \mathcal{SIC}(i,n), (10)\}$$

with $\boldsymbol{pos}$ the UAV position. Note that the search is explicitly over the UAV position, but also implicitly over the power variables which are included in $\mathcal{PMC}(i,n)$, $\mathcal{SIC}(i,n)$. In order to determine the entire region in which TMSIC is guaranteed, one has to:

- Solve the CSP for all 64 combinations. Let r_i be the solution space corresponding to the i^{th} LoS/NLoS configuration, obtained by $r_i = \bigcup_{n=1}^{8} r_{i,n}$.
- The space in which a TMSIC is guaranteed to occur is a region where TMSIC is possible for any channel realization of LoS/NLoS combinations. Therefore, the solution of the CSP shall be obtained by $\mathbb{S} = \bigcap_{i=1}^{8} r_i = \bigcap_{i=1}^{8} \left(\bigcup_{n=1}^{8} r_{i,n} \right)$.

Although these resolution steps provide meaningful insights to the spatial representation of TMSIC-enabled regions, it should be noted that solving these CSPs is done by Set Inversion Via Interval Analysis (SIVIA) [30]. The latter operates on set intervals using the branch-and-prune method, leading to an exponential complexity on the search space dimensions (nine in our case: three UAV position variables and six power variables) and the required resolution error. For our system parameters, the CSP resolution is practically inapplicable. Most importantly, the existence of a TMSIC-guaranteed space region is not guaranteed due to the r_i intersections which may yield an empty space $\mathbb{S}$. In fact, not only TMSIC may not be guaranteed ($\mathbb{S} = \emptyset$), but the regions $r_{i,n}$ themselves might be empty. If $\forall n, r_{i,n} = \emptyset$, then TMSIC cannot be achieved when the i^{th} LoS/NLoS combination occurs. If this is the case for all LoS/NLoS combinations, then TMSIC application is impossible for the considered user triplet and antenna power limits.

While the CSP complexity can be worked around by turning the CSP into an optimization problem, the problem of TMSIC feasibility has to be addressed. Between the extreme cases of impossible TMSIC application and TMSIC-guaranteed application, there is a middle ground in which it is best to assess the TMSIC application in probabilistic terms. To that end, in the next sections the UAV placement problem is first remodeled into an optimization problem, then the probabilistic TMSIC framework is developed.

D. UAV PLACEMENT PROBLEM FORMULATION

It is well known that optimization problems are at the core CSPs associated to an objective function. A family of optimization problems having different objective functions but with the same constraints (the core CSP) leads to different solutions from one another, but within the same solution space of the aforementioned CSP. For the case at hand, setting the optimization problem with the constraints $\mathcal{PMC}(i,n)$, $\mathcal{SIC}(i,n)$ and (10) automatically leads to a solution within the desired region $r_{i,n}$ without requiring the knowledge of the whole region. Let f be the optimization function to be carefully selected by the system administrator, the generic formulation of the UAV placement problem becomes:

$$\begin{aligned} \mathcal{OP}^1_{i,n} : \quad \{\boldsymbol{pos}^*_{i,n}\} = & \underset{\boldsymbol{pos}, P_{k,r}}{\arg\max} f(\boldsymbol{pos}, P_{k,r}), \\ & \text{s.t} : \ \mathcal{PMC}(i,n), \mathcal{SIC}(i,n) \text{ and} \\ & \quad (10) \text{ are verified.} \end{aligned} \tag{11}$$

Then, the best UAV position is retained:

$$\begin{aligned} \{i^*, n^*\} = & \underset{(i,n) \in [\![1..8]\!] \times [\![1..8]\!]}{\arg\max} f(\boldsymbol{pos}^*_{i,n}), \\ \boldsymbol{POS} = & \ \boldsymbol{pos}^*_{i^*,n^*}. \end{aligned} \tag{12}$$

While this approach does not deliver the entire $r_{i,n}$, it guarantees that $\boldsymbol{pos}^*_{i,n}$ is inside $r_{i,n}$. However, if a solution does not exist, then it can be affirmed that $r_{i,n}$ is empty, i.e. TMSIC is impossible to achieve for the combination (i,n). This is true independently of f since the optimization function does not affect the feasibility of the problem that is set by its constraints. Therefore, performing UAV positioning by trying to solve $\mathcal{OP}^1_{i,n}$ for all the combinations is by itself a TMSIC feasibility check. The associated complexity for the resolution of problems of the likes of $\mathcal{OP}^1_{i,n}$ relying on the interior-point method is in $O(l^{2.5})$ [31] where l is the number of variables which is fixed in our case and equal to nine. Therefore, the resolution cost of a single optimization problem will be used hereafter as the reference complexity unit for the complexity comparison of the UAV positioning algorithms.

It is worth mentioning that the knowledge of the $r_{i,n}$ and r_i regions is not assumed, but their use in the discourse is for modeling convenience and for a better understanding of the problem characteristics through a spatial representation of the discussed properties.

In the next section, the probabilistic framework is discussed in order to provide meaningful insights for the selection of the optimization function by the system administrator.

III. PROBABILISTIC FRAMEWORK FOR TMSIC-BASED UAV POSITIONING

To determine the TMSIC probability associated to a UAV position, let $l = 1$ be the value assigned to the state of a LoS link and $l = 0$ to that of a NLoS state. Given the three-bit binary vector (l_1, l_2, l_3) representing the state of the A2G links of users 1, 2, and 3 respectively, we denote by c_i the i^{th} combination that corresponds to its three-bit binary vector in base two plus one, $i = (l_1, l_2, l_3)_2 + 1$. For instance, the all LoS state is represented by c_8, and the all NLoS state is represented by c_1. The space region r_i corresponds then to combination c_i. To define and evaluate the probability of TMSIC for a UAV position, let us consider the probability of achieving TMSIC through c_i:

$$Pr(\text{TMSIC} \cap c_i/\boldsymbol{pos}) = Pr(c_i/\boldsymbol{pos}) \times Pr(\text{TMSIC}/c_i, \boldsymbol{pos}) \tag{13}$$

Analyzing these terms, we state that knowing c_i and $\boldsymbol{pos}$, the probability of having TMSIC is given by:

$$p_i(\boldsymbol{pos}) \triangleq Pr(\text{TMSIC}/c_i, \boldsymbol{pos}) = \begin{cases} 1, \text{if } \boldsymbol{pos} \in r_i & (14) \\ 0, \text{else.} & (15) \end{cases}$$

In other words, for a fixed c_i and a known UAV position, TMSIC is deterministic and not random, it is either feasible or not according to the belonging of $\boldsymbol{pos}$ to r_i. On the contrary, for a fixed UAV position and fixed user positions, c_i is random and any of the eight link states is possible; however, some LoS/NLoS configurations are more likely to occur than others. Since user positions are mutually independent, the probability of having c_i knowing $\boldsymbol{pos}$ is the product of the probabilities of having the channel state of each user matching that of c_i:

$$\begin{aligned} Pr(c_i/\boldsymbol{pos}) &= Pr(l_1/\boldsymbol{pos}) \times Pr(l_2/\boldsymbol{pos}) \times Pr(l_3/\boldsymbol{pos}) \\ &= \prod_{j=1}^{3} \left[l_j P_{\text{LoS}}(\theta_j) + (1 - l_j) P_{\text{NLoS}}(\theta_j) \right], \end{aligned} \tag{16}$$

where $P_{\text{NLoS}}(\theta_j) = 1 - P_{\text{LoS}}(\theta_j)$. Then by applying the law of total probability, the probability of having a TMSIC for a given UAV position is:

$$Pr(\text{TMSIC}/\boldsymbol{pos}) = \sum_{i=1}^{8} Pr(c_i/\boldsymbol{pos}) \times p_i(\boldsymbol{pos}). \tag{17}$$

This clearly shows that the probabilistic nature of TMSIC is bound to the random A2G channel realization and not to the TMSIC procedure itself. Indeed, if the UAV position is fixed, and the LoS/NLoS realization c_j is known, the TMSIC procedure is either possible (for at least one decoding order) or it is not (for any of the decoding orders). Therefore, the UAV position directly affects the TMSIC probability through $Pr(c_i/\boldsymbol{pos})$, provided that $p_i(\boldsymbol{pos}) = 1$, which is translated into the satisfaction of the constraints of $\mathcal{OP}^1_{i,n}$.

We conclude that the TMSIC probability expression in (17) shows that the UAV placement can be made to optimize the TMSIC probability by incorporating this probability into the optimization function f. Based on this fact, the UAV positioning strategies are presented in the next section.

On another hand, once in position, the UAV can determine the actual channel realization c_j through channel estimation by comparing the actual channel gains with the theoretical one in (4). Furthermore, if the obtained c_j is different from the channel realization c_{i^*} that yields $\boldsymbol{POS}$ in (12), not much can be said about the feasibility of TMSIC for c_j. Indeed, the only available information regarding the TMSIC applicability in $\boldsymbol{POS}$ is that $p_{i^*}(\boldsymbol{POS}) = 1$, but $p_j(\boldsymbol{POS})$ is not known. This can only be determined once the UAV position is fixed and the optimization in (11) is rerun for all the decoding orders. This justifies thereby the separation between the UAV placement phase from the power allocation phase which is presented in section V.

IV. PROPOSED UAV POSITIONNING TECHNIQUES BASED ON TMSIC

We present in this section the different strategies that can be used to position the UAV. The approaches that are derived from the LoS/NLoS path loss model are presented first from sections IV-A to IV-C. Alternatively, the approach based on the mean path loss model is presented in section IV-D. In both cases, TMSIC positioning is attempted, if TMSIC turns out to be impossible, a common positioning technique is reverted to in section IV-E.

A. MAXIMUM PROBABILITY POSITIONING (MPP)

In order to maximize the TMSIC probability, the objective function should be set equal to (17). This being said, since the r_i regions cannot be known, then $p_i(\boldsymbol{pos})$ is not available for any UAV position $\boldsymbol{pos}$. This causes a problem to the TMSIC probability expression as we don't know which LoS/NLoS combinations to account for in (17). Nonetheless, following the constraints of $\mathcal{OP}^1_{i,n}$, the only region the UAV is guaranteed to be in after optimization is $r_{i,n}$, thus f is set to $Pr(c_i/\boldsymbol{pos})$ instead of the total TMSIC probability $Pr(\text{TMSIC}/\boldsymbol{pos})$. Therefore, the original optimization using the objective function (17) is replaced by an optimization over a lower bound to (17). The UAV placement problem is then written as follows:

$$\begin{aligned} &\mathcal{OP}^{1,a}_{i,n} : \{\mathcal{OP}^1_{i,n}, f = Pr(c_i/\boldsymbol{pos})\} \\ &\text{s.t} : \ \mathcal{PMC}(i,n), \mathcal{SIC}(i,n) \text{ and (10) are verified.} \end{aligned} \tag{18}$$

The final UAV position is obtained from (12). Given that the remaining combinations ($c_i \neq c_{i^*}$) are not taken into account in $Pr(\text{TMSIC}/\boldsymbol{POS})$, the computed TMSIC probability $Pr(c_{i^*}/\boldsymbol{POS})$ is only a lower bound to the actual TMSIC probability $Pr(\text{TMSIC}/\boldsymbol{POS})$. The obtained lower bound achieves optimality when $Pr(\text{TMSIC}/\boldsymbol{POS})$ equals to $Pr(c_{i^*}/\boldsymbol{POS})$, in other words when $\boldsymbol{POS} \in r_{i^*}$ and $\boldsymbol{POS} \notin \cup_{i=1, i\neq i^*}^{8} r_i$. However, since the combination c_{i^*} leading to $\boldsymbol{POS}$ is not known in advance, the only situation where the solution to $\mathcal{OP}^{1,a}_{i,n}$ is guaranteed to achieve optimality is when the r_i regions are pairwise disjoint.

B. MAXIMUM RATE POSITIONING (MRP)

When solving $\mathcal{OP}_{i,n}^{1,a}$, the obtained UAV position guarantees the best TMSIC probability without taking into account the resulting achievable throughput. Another approach to UAV positioning is based on the maximum achievable throughput via TMSIC. That way, if a UAV position enabling TMSIC exists for the given user cluster, both MPP and MRP deliver UAV positions enabling TMSIC, but with different values of the associated throughput and the lower bound on TMSIC probability. Let $R_{TMSIC} = \sum_{k=1}^{3} R_k$ be the total throughput achieved when TMSIC is enabled. The MRP problem takes the following form:

$$\begin{aligned} &\mathcal{OP}_{i,n}^{1,b} : \{\mathcal{OP}_{i,n}^{1}, f = R_{TMSIC}\} \\ &\text{s.t}: \ \mathcal{PMC}(n,i), \mathcal{SIC}(n,i) \text{ and (10) are verified,} \end{aligned} \quad (19)$$

and the final UAV position is obtained from (12).

C. MAXIMUM PROBABILITY AND RATE POSITIONING (MPRP)

In section IV-A, the position obtained through MPP yields the best TMSIC probability; however, it does not hold any guarantee with regards to the achievable throughput. In contrast, when the system throughput is favored, the results may give UAV positions with high throughput but poor TMSIC probability. Therefore, instead of aiming at maximizing the chances of TMSIC or the system throughput alone, the UAV is positioned such that the product of the rate by the associated probability is maximized:

$$\begin{aligned} &\mathcal{OP}_{i,n}^{1,c} : \{\mathcal{OP}_{i,n}^{1}, f = Pr(c_i/\boldsymbol{pos})R_{TMSIC}\} \\ &\text{s.t}: \ \mathcal{PMC}(n,i), \mathcal{SIC}(n,i) \text{ and (10) are verified.} \end{aligned} \quad (20)$$

Compared to other UAV positioning techniques seeking TMSIC, this approach has the advantage of accounting for both the throughput associated to a combination c_i, as well as its probability of occurence. On the other hand, the obtained position does not favor TMSIC as much as MPP solutions. Another approach to position the drone relying on the mean path loss instead of the LoS/NLoS combination is developed next as an alternative to MPP, MRP and MPRP.

D. MEAN PATH LOSS POSITIONING (MPLP)

Most works on flying base stations [4], [23], [32] are based on the mean path loss of A2G channels to perform scheduling tasks. The mean path loss of A2G links is given by:

$$L_{av} = P_{\text{LoS}} L_{\text{LoS}} + P_{\text{NLoS}} L_{\text{NLoS}}. \quad (21)$$

The A2G links in this case are no longer defined by the three-bit vector (l_1, l_2, l_3) of LoS/NLoS combinations. The whole concept of LoS/NLoS combinations (c_i) and regions (r_i) becomes irrelevant since a unique expression is available for every user-UAV link. Therefore, the PMC and SIC conditions depend only on the decoding order, hence the notations $\mathcal{SIC}(n), \mathcal{PMC}(n)$. Achieving TMSIC cannot be formulated as a probability maximization problem that depends on the different LoS/NLoS combinations: for the given user triplet, either TMSIC is achieved or it is not. However, to avoid running into another CSP, we consider the system throughput objective function and search for the UAV position that maximizes it as follows:

$$\begin{aligned} &\mathcal{OP}_{n}^{2} : \ \{\boldsymbol{pos}_n^*\} = \arg\max_{\boldsymbol{pos}, P_{k,r}} (R_{TMSIC}) \\ &\text{s.t}: \ \mathcal{SIC}(n), \mathcal{PMC}(n), \textit{and}(10) \text{ are verified.} \end{aligned} \quad (22)$$

Even though the objective function does not compromise the feasibility of the solution in any way (no additional constraints are involved), it affects the position of the UAV and therefore the performance of the obtained solution in terms of achieved TMSIC probability and throughput. In fact, this issue is not specific to rate maximization, i.e. any other objective function would have been the subject of the same inconvenience. The reason for that is the use of an average channel model to obtain the UAV position. Having obtained the drone position for every decoding order (when the system admits a solution), the position yielding the maximum value of the objective function is selected:

$$\begin{aligned} \{n^*\} &= \arg\max_{n \in [\![1..8]\!]} (R_{TMSIC}), \\ \boldsymbol{POS} &= \boldsymbol{pos}_{n^*}^*. \end{aligned} \quad (23)$$

When comparing the procedure for the $\boldsymbol{POS}$ assignment in (23) to the procedure used for MPP, MRP and MPRP in (12), an eight-fold complexity decrease is observed using the mean path loss model in MPLP. The 64 combinations of decoding orders and LoS realizations that required solving turn into 8 combinations of the unique channel realization - the mean path loss channel - with the decoding orders. This difference will be accounted for when discussing the selection of the best UAV positioning technique in the performance assessment (section VI).

E. PROBABILISTIC APPROACH BASED ON SUB-BAND SPLITTING POSITIONING (SSP)

When TMSIC proves to be impossible (cf. section II-D) an alternative UAV positioning technique can be used. Some of its desirable properties are the guarantee of obtaining a solution for any user positions and a reduced complexity compared to TMSIC. In [22], [33], mutual (dual) SIC between two users (DMSIC) on the same sub-band was shown to be always possible when serving the users with two different BSs. Therefore, in case of TMSIC impossibility, we propose to divide the sub-band into two equal half sub-bands (supposed to have equal channel gains), and then to pair the cell-edge user (user 3 of Fig. 1) with one of the cell-center users (user 1 or user 2 of Fig. 1) on each half sub-band. This leads to two independent pairs of users applying DMSIC separately on each sub-band. Their PMCs are:

PMCs for DMSIC between (U_1, U_3)

$$\begin{cases} P_{3,1,1}h_{1,1} + P_{3,2,1}h_{1,2} > P_{1,1,1}h_{1,1} + P_{1,2,1}h_{1,2} \\ P_{1,1,1}h_{3,1} + P_{1,2,1}h_{3,2} > P_{3,1,1}h_{3,1} + P_{3,2,1}h_{3,2} \end{cases} \quad (24)$$

PMCs for DMSIC between (U_2, U_3)

$$\begin{cases} P_{3,1,2}h_{2,1} + P_{3,2,2}h_{2,2} > P_{2,1,2}h_{2,1} + P_{2,2,2}h_{2,2} \\ P_{2,1,2}h_{3,1} + P_{2,2,2}h_{3,2} > P_{3,1,2}h_{3,1} + P_{3,2,2}h_{3,2} \end{cases} \quad (25)$$

where the additional index d in the power terms $P_{k,r,d}$ refers to the used half sub-band. Users 1 and 3 are paired on the first half sub-band ($d = 1$), and users 2 and 3 are paired on the second half sub-band ($d = 2$). Note that DMSIC constraints are met when the PMCs are satisfied, as it was proven in [22]. Moreover, a single decoding order is possible at the level of every user in the respective half sub-band, hence the positioning problem needs to be solved only once for every c_i. Then, similarly to MPRP, the UAV placement aims at maximizing the product of the DMSIC throughput by the c_i probability. The following problem is solved for the eight c_i channel realizations and then the resulting position of the combination leading to the highest value is selected.

$$\begin{aligned} &\mathcal{OP}_i^3 : \{\boldsymbol{pos}\}^* \\ &= \underset{\boldsymbol{pos}, P_{k,a,m}}{\arg\max} \left(R_{DMSIC} \times Pr(c_i/\boldsymbol{pos})\right), \\ &\quad \text{s.t} : (24), (25) \text{and} \\ &\qquad \begin{cases} P_{1,1,1} + P_{2,1,2} + P_{3,1,1} + P_{3,1,2} \leq P_{L_1} \\ P_{1,2,1} + P_{2,2,2} + P_{3,2,1} + P_{3,2,2} \leq P_{L_2}, \end{cases} \end{aligned} \quad (26)$$

where the system throughput R_{DMSIC} is given by:

$$\begin{aligned} R_{DMSIC} = &\sum_{k\in\{1,3\}} \frac{B}{2} \log_2 \left(1 + \frac{\sum_{r=1}^{2} P_{k,r,1}h_{k,r}}{N_0 B/2}\right) \\ &+ \sum_{k\in\{2,3\}} \frac{B}{2} \log_2 \left(1 + \frac{\sum_{r=1}^{2} P_{k,r,2}h_{k,r}}{N_0 B/2}\right) \end{aligned} \quad (27)$$

This positioning technique is only used when the chosen TMSIC positioning technique (MPP, MPRP, or MPLP) fails to provide a solution.

V. POWER ALLOCATION STRATEGY

We present hereafter the global PA approach that is applied at the level of the BS of cell 1 and instructed to the UAV to maximize system throughput. The approach resides in applying TMSIC when possible, otherwise alternative non-TMSIC PAs are used. In the following, we detail how the global PA approach is adapted according to the alternative power allocation technique (APAT) and the UAV positioning technique (UPT). The flow chart describing the complete power allocation strategy is presented in Fig. 2.

It was discussed, in section II-D, that performing UAV positioning by trying to solve the variants of $\mathcal{OP}_{i,n}^1$ is a TMSIC feasibility check. Through that check, empty $r_{i,n}$ regions are determined. If all the regions are empty, i.e. if no UAV position is obtained, the check fails and the non-TMSIC PAs of section V-B are applied. If a UAV position is obtained, then TMSIC PA might be feasible, thus TMSIC PA is attempted.

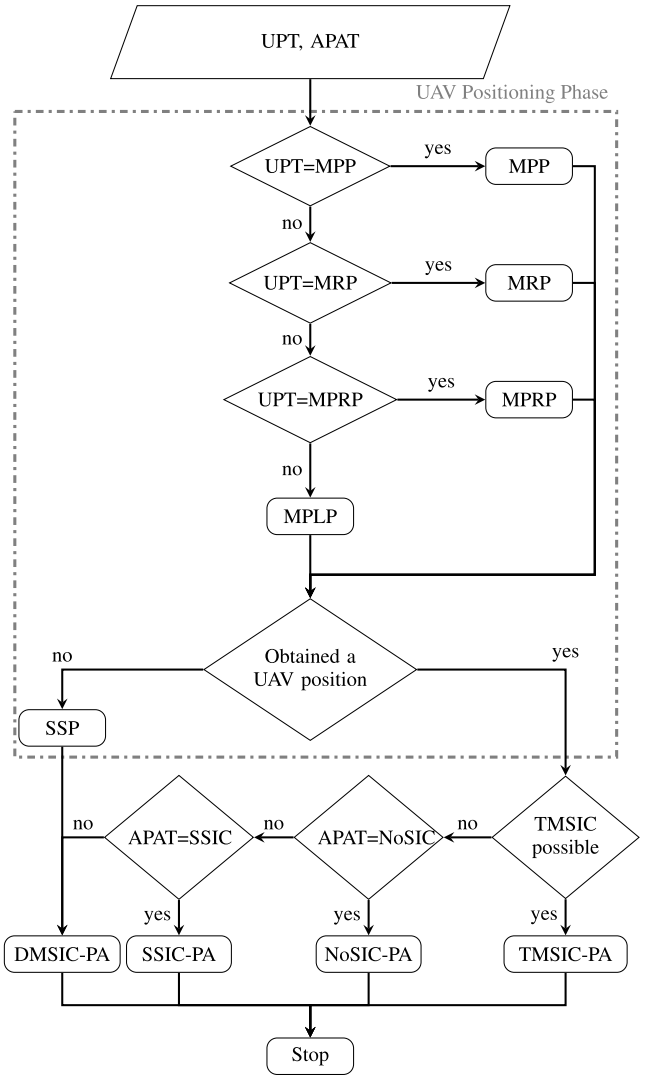

FIGURE 2. Flow chart of the global strategy for the different UPT-APAT pairs selected by the system administrator.

A. TMSIC PA AND TMSIC TESTING

If a UAV position is obtained, three cases are identified according to three quantities:

- c_{i^*}, the channel realization which leads to ***POS***,
- c_j, the actual channel realization obtained after positioning the UAV,
- $\mathcal{N}$, the set of decoding orders for which $r_{j,n}$ exists is non empty.

The three cases are:

1) $c_j = c_{i^*}$: TMSIC-PA is feasible, and the PA problem $\mathcal{OP}_{j,n}^4$ is solved for the decoding orders in $\mathcal{N}$ (which cannot be empty).
2) $c_j \neq c_{i^*}, \mathcal{N} \neq \emptyset$: TMSIC-PA might be feasible, and we need to solve $\mathcal{OP}_{j,n}$ for $n \in \mathcal{N}$ to check its feasibility.
3) $c_j \neq c_{i^*}, \mathcal{N} = \emptyset$: TMSIC-PA is not feasible; in this case, we must revert to non-TMSIC PAs (section V-B).

Note that, once the UAV is positioned, the PA does not affect the TMSIC probability, and so the optimization function is the same for MPP, MRP, MPRP and MPLP which is throughput

maximization:

$$\mathcal{OP}^4_{j,n}: \quad \{P^*_{k,r}\} = \arg\max_{P_{k,r}} \left(R_{TMSIC}\right),$$
$$\text{s.t}: \mathcal{PMC}(j,n), \mathcal{SIC}(j,n) \text{ and (10) are verified.} \quad (28)$$

In the second case, achieving TMSIC is not guaranteed because ***POS*** might be outside of the $r_{j,n}$ ($n \in \mathcal{N}$) regions. That is why, $\mathcal{OP}^4_{j,n}$ needs to be solved to determine if TMSIC is feasible. For the case of MPLP, the existence of the $r_{i,n}$ regions has not been tested during the UAV positioning phase (as for MPP, MRP and MPRP), hence $\mathcal{OP}^4_{j,n}$ is solved/checked for all the decoding orders. These differences are pictured in Fig. 3.

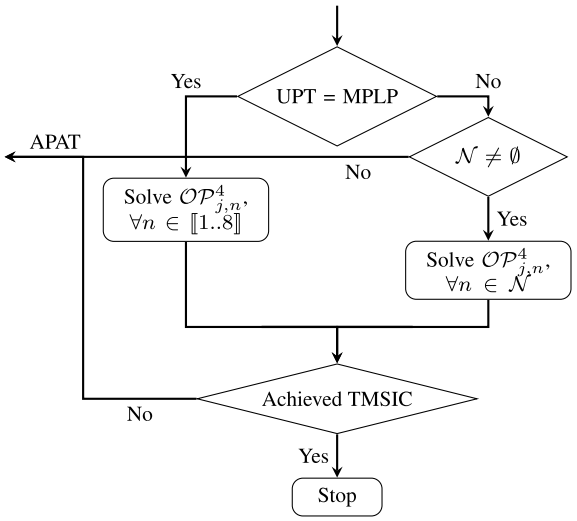

FIGURE 3. Detailed flow chart of the testing and the TMSIC-PA blocks of Fig. 2.

B. ALTERNATIVE POWER ALLOCATION TECHNIQUES

In the case where TMSIC is not feasible, several PA alternatives for system throughput maximization are possible. Based on the principle that the achieved rate increases when interference cancellation is successfully conducted, it is natural to seek the highest number of SIC procedures between the three users. Since TMSIC corresponds to 6 SICs, two at the level of each user, when one SIC fails, we can apply a 5-SIC procedure. Following this pattern, 5 SICs, than 4, 3, 2 and a single SIC must be all tried in that order until the first setup that leads to a valid PA solution. This ideal strategy counts 112 potential problems to be solved when taking into account all possible decoding orders for every case. Due to the number and complexity of these problems, this strategy is disregarded. Besides, the success of this strategy is not guaranteed, just like it was not the case for TMSIC. Three alternative non-TMSIC PAs are proposed. When a TMSIC procedure is declared infeasible after undergoing the tests in section V-A, the BS of cell 1 executes one of the following PA schemes:

1) DMSIC

Following the reasoning of section IV-E, we resort to sub-band division followed by DMSIC, with the difference that DMSIC is now used for PA and not for UAV positioning. The DMSIC-PA problem takes the following form:

$$\mathcal{OP}^{5,a}: \quad \{P_{k,r,d}\}^* = \arg\max_{P_{k,r,d}} \left(R_{DMSIC}\right), \quad (29)$$

such that the constraints of $\mathcal{OP}^3_i$ are verified. Since the UAV position has been fixed previously, $\mathcal{OP}^{5,a}$ is solved only once for the obtained configuration c_j (unlike $\mathcal{OP}^3_i$ that is solved for all combinations in section IV-E) and the resulting power allocation is instructed to the UAV by the BS.

2) NoSIC

Without dividing the sub-band, a simpler alternative to TMSIC resides in abandoning all SIC procedures and optimizing the new rate maximization problem without any other system constraints than the total transmit power of BSs. Users signals interfere on one another and the problem formulation is given by:

$$\mathcal{OP}^{5,b}: \{P_{k,r}\}^* = \arg\max_{P_{k,r}} \left(\sum_{k=1}^{3} B \log_2\left(1 + \frac{\sum_{r=1}^{2} P_{k,r} h_{k,r}}{\sum_{k'=1,k'\neq k}^{3} P_{k',r} h_{k',r} + N_0 B}\right)\right)$$
$$s.t.(10) \text{ is satisfied.} \quad (30)$$

3) SINGLE SIC (SSIC-PA)

Standard NOMA SIC procedures may also be used when TMSIC is impossible. In this case, the strong users in the two cells, i.e. U1 and U2, successfully decode the signal of the weak user U3 that cannot perform SIC. This interference cancellation scheme is similar to the NOMA-CoMP system adopted in [34], with the difference that in our system all users are served through JT-CoMP (and not only the cell-edge user). The corresponding optimization problem is:

$$\begin{aligned}\mathcal{OP}^{5,c}: \{P_{k,r}\}^* = \arg\max_{P_{k,r}} \Bigg[& B\log_2\left(1 + \frac{P_{1,1}h_{1,1} + P_{1,2}h_{1,2}}{P_{2,1}h_{1,1} + P_{2,2}h_{1,2} + N_0 B}\right) \\ & + B\log_2\left(1 + \frac{P_{3,1}h_{3,1} + P_{3,2}h_{3,2}}{(P_{1,1}+P_{2,1})h_{3,1} + (P_{1,2}+P_{2,2})h_{3,2} + N_0 B}\right) \\ & + B\log_2\left(1 + \frac{P_{2,1}h_{2,1} + P_{2,2}h_{2,2}}{P_{1,1}h_{2,1} + P_{1,2}h_{2,2} + N_0 B}\right)\Bigg] \end{aligned} \quad (31)$$

such that:

- SIC of the signal of U3 is guaranteed at the level of U1 and U2 respectively:
  $(h_{1,1}h_{3,2} - h_{1,2}h_{3,1})[P_{3,1}(P_{2,2} + P_{1,2}) - P_{3,2}(P_{1,1} + P_{2,1})] > 0$
  $(h_{2,1}h_{3,2} - h_{2,2}h_{3,1})[P_{3,1}(P_{2,2} + P_{1,2}) - P_{3,2}(P_{1,1} + P_{2,1})] > 0$
- PMC constraints are verified at the level of U1 and U2 respectively:
  $P_{3,1}h_{1,1} + P_{3,2}h_{1,2} > (P_{1,1} + P_{2,1})h_{1,1} + (P_{2,2} + P_{1,2})h_{1,2}$
  $P_{3,1}h_{2,1} + P_{3,2}h_{2,2} > (P_{2,2} + P_{1,2})h_{2,2} + (P_{1,1} + P_{2,1})h_{2,1}$
- Power limit constraints are satisfied as in (10).

Note that the SIC and PMC derivations for this case are directly deduced from [22] (section V-A), where they were developed for the case of JT at UE3. It was noted there that the common power factor in the SIC conditions implies an identical sign of the channel terms: $\text{sign}(h_{1,1}h_{3,2}-h_{1,2}h_{3,1}) = \text{sign}(h_{2,1}h_{3,2} - h_{2,2}h_{3,1})$. If the users channel gains do not comply with this condition, the single SIC procedure cannot work, and the PA scheme reverts to NoSIC-PA.

As stated in the beginning of this section, the first aim of the presented PA procedures is the accomplishment of a successful TMSIC. In other words, APAT is applied as a backup solution just like SSP was for MPP, MRP, MPRP and MPLP. In the performance assessment section, the nomenclature of the resource allocation techniques is done according to the selected TMSIC-based positioning, and to the selected APAT.

VI. PERFORMANCE ASSESSMENT PROCEDURE AND SIMULATION RESULTS

A. PERFORMANCE ASSESSMENT

In the previous section, the global PA strategy was detailed to determine the throughput associated to a given user combination. As already explained, even when the users positions are fixed and the UAV position has been found, c_j cannot be determined in advance before placing the UAV and measuring the obtained A2G links. Due to the random nature of LoS/NLoS links, any combination can occur and a fair comparison in the simulation results can only be made when the throughput associated to the UAV position is averaged over all possible combinations. Section V presented the PA steps followed at the level of the BS a_1 in real time, whereas this section presents the followed procedure to simulate and assess the performance of each UPT-APAT couple. Let $\mathcal{R}$ be the rate vector associated to every combination c_i; the expected achieved rate for the determined UAV position is given by:

$$\overline{R} = \sum_{i=1}^{8} \mathcal{R}(i) Pr(c_i/\boldsymbol{POS}) \tag{32}$$

To estimate $\mathcal{R}$, the procedure followed in section V (sections V-A and V-B successively) is iterated for every channel combination. By doing so, the TMSIC testing procedure (Fig. 3) is undergone for every c_i, and the probability $p_i(\boldsymbol{POS})$ of having TMSIC (or not) knowing c_i and $\boldsymbol{POS}$ is determined. Thus, the exact TMSIC probability is retrieved from (17).

B. SIMULATION RESULTS

To evaluate the performance of the presented UPTs and APATs, 1000 simulations are conducted with different positioning of the users according to Fig. 1. The outer cell radius of each hexagonal cell is $R_d = 500$ m. The user 3 region has a maximum width of 60 m along the x axis. Users are assumed to have low mobility, they are independently positioned, their positions being randomly generated with a uniform probability distribution over their respective regions. The transmission channel model between the fixed BS and the users includes a distance-dependent path loss of decay factor 3.76, and a zero-mean lognormal shadowing with an 8 dB variance. The working frequency is 2 GHz, and the parameters of the A2G model are $\alpha = 9.61$, $\beta = 0.16$, $\eta_{LoS} = 1$ dB and $\eta_{NLoS} = 19$ dB, corresponding to an urban environment [25]. The search region for UAV positioning is a rectangular box delimited along the x axis by the cell diameters at the edges of regions 1 and 2 respectively, with the UAV height varying between 50 m and 100 m above the ground. The considered sub-band bandwidth is $B = 156.25$ kHz (equivalent to a total bandwidth of 10 MHz subdivided into 64 sub-bands). The power spectral density of the additive background white noise is $N_0 = -174$ dBm/Hz, and the noise power in a sub-band is $\sigma^2 = N_0 B$. The power limit constraint over the fixed BS (a_1) is varied between 0.5 W and 5 W, and the MBS power limit assigned to the user cluster is 0.5 W. MATLAB software is used to generate the numerical results and *fmincon* from the optimization toolbox is used to solve the optimization problems in each proposed technique.

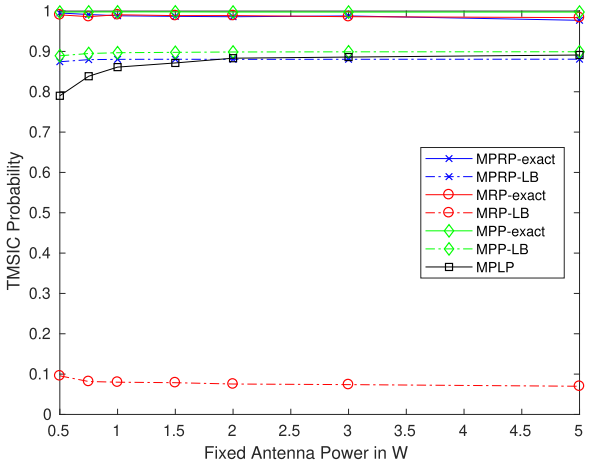

FIGURE 4. TMSIC probability of the UAV positioning techniques as a function of the fixed antenna power P_{L_1}.

The TMSIC probability of the UAV positioning techniques is independent of the used APATs, hence the methods presented in Fig. 4 are named after the UPT. The Lower Bound (LB) curves of MPP, MRP and MPRP represent the probability of achieving TMSIC through c_{i^*}, $Pr(c_{i^*}/\boldsymbol{POS})$. The exact probability curves add to the LBs the probability of other combinations that enable TMSIC when the UAV is in $\boldsymbol{POS}$. As expected, MPP-LB delivers the best TMSIC probability between the three methods with 89.9% TMSIC success rate, with MPRP coming second with 88%, and MRP is last with 6.9% for $P_{L_1} = 5$ W. This important deficit in probability of MRP compared to the two other methods is explained by the absence of the probability term in its objective function: the UAV position is selected according to the throughput it could provide irrespective of the associated probability. This being said, the probability that truly matters is the exact probability, since it reflects the experienced TMSIC probability. We first point out the remarkable closeness between MPP, MRP and MPRP-exact despite the relatively important differences in the lower bounds. While a

10% increase in the TMSIC success rate of MPP and MPRP due to the contribution of the remaining configurations is an intuitive result, it is less evident to explain the substantial increase in probability observed for MRP (from 6.9% to 98%). In fact, the small lower bound probability for MRP translates into a low probability of occurrence of c_{i^*}, then other configurations have higher probabilities of occurrence. If these lead to a TMSIC, their contribution to the total probability will be dominant with respect to c_{i^*}. This was confirmed by a statistical analysis of the number of configurations leading to TMSIC per simulation, which showed that, on average, 7.68 configurations out of the eight yield a TMSIC for MRP. The same analysis can be transposed to MPLP, since it does not account for the TMSIC probability when positioning the MBS (the technique is transparent to the LoS/NLoS combination paradigm). Nevertheless, an average of seven combinations out of the eight enable TMSIC, which explains the relatively high TMSIC probability 89.1%. However, this probability is the lowest among that of all UPTs.

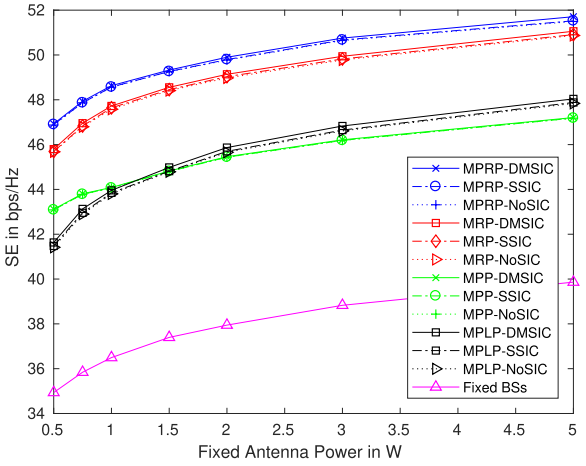

FIGURE 5. Spectral efficiency of the different UAV positioning techniques and PA strategies.

Fig. 5 shows a comparison of the system performance in terms of the average SE for all PA and positioning techniques. The achieved SE when the two fixed BSs are available to serve users is added for comparison; DMSIC is used as PA in this case. The performance improvement due to the UAV mobility, compared to fixed BSs, is clearly observed for all the positioning techniques. Also, the consideration of LoS/NLoS combinations efficiently improves the SE by 3 to 5 bps/Hz for MRP and MPRP compared to MPLP. However, the average MPP performance is lacking behind, as it only surpasses MPLP for small P_{L_1} values before switching orders for power limit values above 1.5 W. This suggests that the evolution of the UAV position with the growing value of P_{L_1} affects the A2G links in a way that the increase rate of the MPP throughput is lower than that of MPLP. Indeed, an analysis of the UAV positioning in MPP and its evolution with the power limit show that high P_{L_1} values tend to place the UAV at the edges of the search region, resulting in poor channel gains, which explains the lower throughput compared to MPLP at $P_{L_1} = 5$ W. More details on the reasons behind

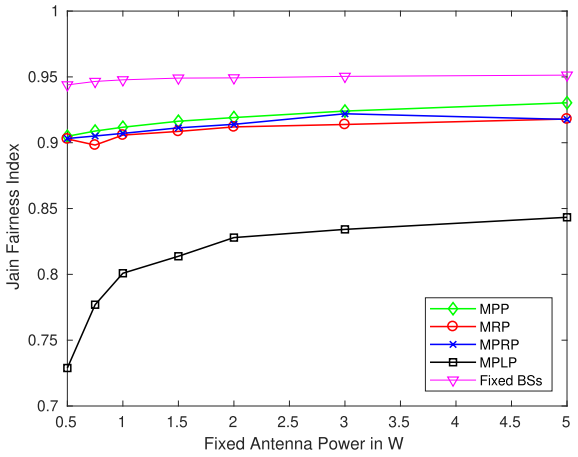

FIGURE 6. Fairness comparison of the positioning techniques as a function of the fixed antenna power.

this placement, its interaction with the user positioning and the effect it has on the user throughput are given later for all the positioning techniques in the analysis of the individual user rates shown in Fig. 7.

Nonetheless, we can sum up the results of Fig. 5 by stating that focusing exclusively on the TMSIC probability can mislead the UAV placement into areas with poor A2G links and poor achievable throughput. The introduction of the throughput in the objective function provides the qualitative edge for MRP over MPP, since throughput is accounted for during positioning, while the TMSIC probability difference between the two is negligible (cf. Fig. 4). This being said, combining the throughput and the probability in MPRP provides even better results since both objectives are accounted for from the start of the positioning process. However, this performance gain of MPRP and MRP comes at the cost of an additional complexity compared to MPLP, since 64 combinations need to be checked for MRP and MPP compared to the eight decoding orders assessed by MPLP.

Regarding the NoSIC, SSIC, and DMSIC APAT variants for every UPT, small performance differences are observed for all techniques. This is due to the fact that, most of the time, TMSIC is successfully applied and non-TMSIC PAs are summoned for only a small proportion of LoS/NLoS combinations not leading to a TMSIC (around 0.3/8 or less for all UPTs when $P_{L_1} = 0.5$ W). Nonetheless, DMSIC is the best APAT in terms of throughput and is therefore used by default from hereinafter. The methods names are selected according the selected UPT in the following results.

In Fig. 6, the Jain fairness index [35] is used to assess the fairness of the contribution of each user to the total throughput. The index is upper bounded by 1 for absolute fairness and lower bounded by 1/3 for the worst case scenario. It is first observed that MPLP presents the lowest fairness index with a maximum of 0.84 for $P_{L_1} = 5$ W. The other techniques present much higher fairness indices. This is due to the significantly higher probability of achieving TMSIC which is known to provide better throughput through better fairness [22], by ensuring that all users remove their

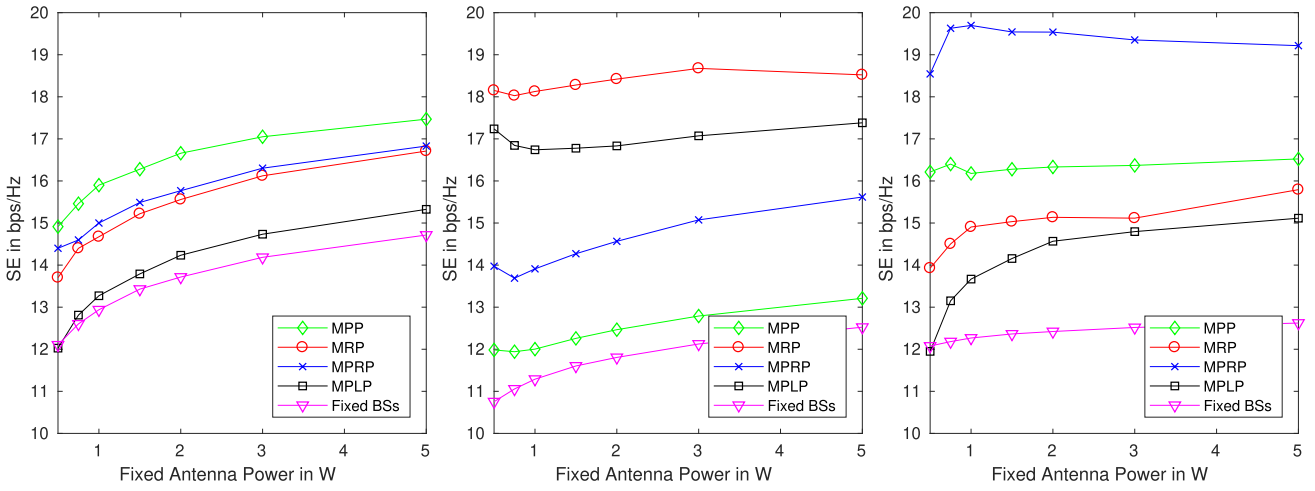

(a) User 1 (b) User 3 (c) User 2

FIGURE 7. Throughput distribution over the three-user NOMA cluster.

respective interference. The remaining UPTs have a quite similar fairness, with the MPP presenting an overall better fairness, especially for high P_{L_1} values. The fixed BSs scenario presents a slightly better fairness compared to MPP, MRP and MPRP. In fact, as in MPP where the UAV placement is pushed back towards the limit of the search region for high power limits, the fixed BSs correspond to a_2 being further away from the user cluster, compared to other UPTs. This translates into a smaller achieved throughput, as shown in Fig. 5, but it also leads to a greater fairness due to the symmetry of the user cluster with respect to a_1 and old a_2.

So far MPP has been shown to provide the best TMSIC probability and fairness from Figs. 4 and 6, whereas MPRP was shown to yield the highest sum-throughput in Fig. 5. Although a trade-off does exist between throughput and fairness, the closeness of the fairness measures and TMSIC probability between MPRP and MPP (0.03 units of difference in the fairness index, and one percentage point difference in probability), compared to the large gap in throughput (around 4.5 bps/Hz, i.e. a 10% difference) does tend to promote MPRP as the best trade-off. However, when having a closer look at the individual user rates for every UPT, other factors come into play which affect the choice of the positioning technique as seen from the results of Fig. 7.

In Fig. 7, we present the individual throughput of every user category, for all positioning techniques. The separate contribution of each user in the cluster throughput is analyzed for each UPT. Starting with the two fixed BSs, we can observe that the influence on throughput of the growing power limit is more pronounced for user 1 than for user 3, and for user 3 more than for user 2. The closer the user is to a_1 on average, the more it benefits from the additional power of a_1. However, user 3 globally presents the lowest user throughput in the cluster, because of its geographical position on the cells edges.

To analyze the performance of positioning techniques, we must first discuss the effect of the UAV position on the channel gains as well as how the objective functions affect this position. We start by focusing on the TMSIC probability as objective function. According to (3), the LoS link with user k has its chances maximized when θ_k tends to 90° (the UAV is on top of k), and the NLoS link is favored when θ_k tends to 0° (the UAV and k are far apart on the xy plane). If the users are (very) close to one another, then placing the UAV on top of the three of them leads to the largest c_8 probability (the all-LoS case). If not, the c_is achieving the best probability are when the UAV is placed almost at the top of one user, establishing a LoS link with that user and favoring NLoS links with the other two. In that scenario, user 3 is the least likely to have the UAV on top of it: being a cell-edge user, the distance separating it from the other two users (which would be the distance separating them from the UAV in the xy plane) is rather small compared to the distance that separates user 1 from user 2 if the UAV was placed on top of one of these two. This smaller distance reduces the chances of NLoS with users 1 and 2 when the UAV is on top of user 3, that is why c_5 and c_3 are favored (i.e. either user 1 or user 2 being in LoS). This explains why the rate of user 3 in MPP is below those of user 1 and 2, with an average rate difference of 4 bps/Hz. Also, if the users are far enough from one of the corners of the search region, the all-NLoS combination (c_1) becomes the most probable combination, under the condition of a possible TMSIC for the UAV position at this corner. This is aided by the growing power limit which enables more locations to achieve TMSIC. However, placing the UAV at the corners of the search region with higher powers induces poorer channel gains due to the free space path loss and to the high NLoS probability, which explains the behavior of MPP in Fig. 5.

When the throughput is considered in the objective function, a significant advantage is given for user 3 over users 1 and 2 because of its location in between the two cell-center users. When only the throughput is considered (as in MRP and MPLP), LoS dominant combinations are favored due to their better channel gains yielding a better throughput.

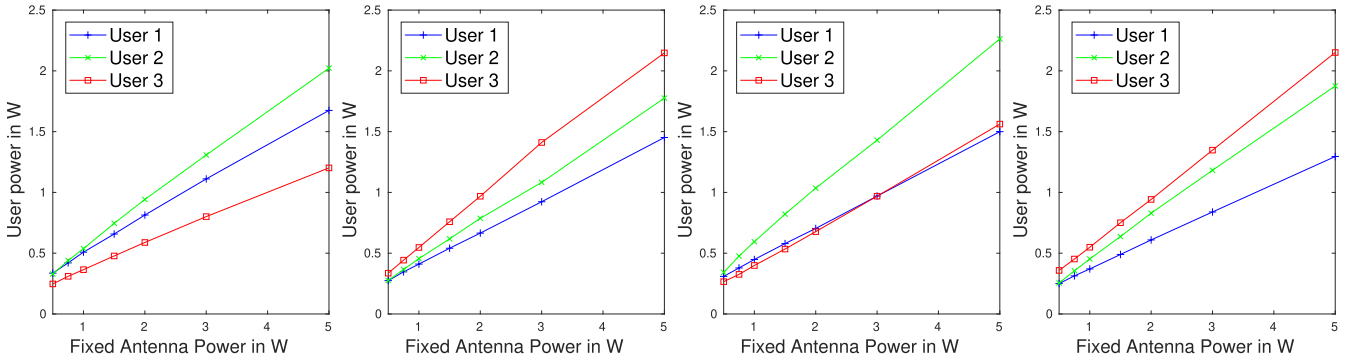

(a) MPP (b) MRP (c) MPRP (d) MPLP

FIGURE 8. User power allocation according to the selected UPT.

However, for the resulting position, the combination which yielded the UAV position is rarely the most favorable one (as discussed previously for Fig. 4) and the actual combination contributing the most to the TMSIC probability is c_2. In other terms, the UAV ends up in between the three users, favoring thereby a LoS link only with user 3, enhancing its rate as shown in Fig. 7 for both MPLP and MRP. Regarding MPRP, the fact that it takes into account both throughput and probability enabled it to deliver the best solutions from the average throughput perspective. Such solutions usually reside in placing the UAV relatively close to user 2 (by favoring c_3) so that the system throughput is maximized. Obviously, doing so profits most to user 2: its average rate is around 19 bps/Hz when user 1 and user 3 rates vary between 14 and 16 bps/Hz.

The presented results from Fig. 7 can also be looked at from the perspective of the average power allocated to each user for every UPT. It can be seen from Figs. 8b and 8d that rate-focused techniques like MRP and MPLP, which tend to place the UAV over user 3 (favoring c_2), end up loading user 3 with the highest power level, translating into a higher throughput of user 3 compared to users 1 and 2. On the other hand, it is also clear from Figs. 8a and 8c for MPP and MPRP that the power allocated to users 1 and 2 is more important than for user 3. As mentioned previously for Fig 7 regarding these methods, the UAV placement favors UAV locations over user 1 (c_5) and user 2 (c_3), leading to a higher achieved throughput for users 1 and 2 compared to user 3. More so, since MPRP favors c_3 exclusively, a greater gap is observed between the powers of user 1 and user 2 in MPRP compared to MPP. In fact, combining the analyses of Figs. 7, 8a and 8c, we can say that MPP delivers similar rate and power allocations to users 1 and 2 with user 3 lacking behind, whereas MPRP delivers similar rate and power allocations to users 1 and 3 with user 2 ahead of both users.

This great diversity in the performance results at the level of every different user provides a broad selection choice depending on system priorities. If cell-edge user's performance is prioritized (and thereby cell-edge user groups) over the total system throughput, going with MRP is the most suitable choice. On the other hand, if cell-center user's performance is the priority, then MPRP and MPP can be employed in such cases, while keeping in mind that MPRP delivers the best overall throughput performance. Finally, MPLP can be also used to favor the cell-edge user, while maintaining a good global throughput and also reducing the optimization complexity compared to MRP due to the simpler mean path loss model. This wide panel of selection also provides the network planner with a multitude of answers to face the variations in time of the users traffic requirements, where the user priorities could change and therefore the UPT strategy can change accordingly.

VII. CONCLUSION

In this work, we addressed the problem of UAV placement for supporting an overloaded BS in a two-cell NOMA CoMP system. The UAV positioning seeks the application of TMSIC which provides great fairness and throughput performance. The proposed approach considers the LoS/NLoS channel combinations of users, instead of using the mean path loss, which proved its efficiency in both TMSIC probability and system throughput. Exclusive attention to TMSIC probability over system throughput showed its shortcomings regarding high power limit values, whereas the combination of probability and throughput information best captures the features of the problem and delivers the best performance results. The presented techniques have a great diversity and can be selected at will according to which group of users is prioritized (cell-edge vs. cell-center) with negligible compromise on system performance.

APPENDIX A
DERIVATION OF THE MUTUAL SIC CONDITIONS

The SINR condition for the decoding of s_n at the level of p is: $SINR_p^{s_n} > SINR_n^{s_n}$. By subtracting $SINR_n^{s_n}$ from $SINR_p^{s_n}$ we get:

$$SINR_p^{s_n} - SINR_n^{s_n} = \frac{P_{n,1}h_{p,1} + P_{n,2}h_{p,2}}{\sum\limits_{i \in \mathcal{I}_{pn}^{s_n}} (P_{i,1}h_{p,1} + P_{i,2}h_{p,2}) + \sigma^2} - \frac{P_{n,1}h_{n,1} + P_{n,2}h_{n,2}}{\sum\limits_{i \in \mathcal{I}_{pn}^{s_n}} (P_{i,1}h_{n,1} + P_{i,2}h_{n,2}) + \sigma^2} > 0$$

which leads to

$$A = (P_{n,1}h_{p,1} + P_{n,2}h_{p,2})\Big[\sum_{i\in\mathcal{I}_n^{s_n}}(P_{i,1}h_{n,1} + P_{i,2}h_{n,2}) + \sigma^2\Big]$$
$$-(P_{n,1}h_{n,1}+P_{n,2}h_{n,2})\Big[\sum_{i\in\mathcal{I}_p^{s_n}}(P_{i,1}h_{p,1}+P_{i,2}h_{p,2})+\sigma^2\Big] > 0,$$

where A is the numerator of $SINR_p^{s_n} - SINR_n^{s_n}$, its expression can be further rearranged as:

$$\begin{aligned} A = {} & h_{n,1}h_{p,1}P_{n,1}\Big[\sum_{i\in\mathcal{I}_n^{s_n}}P_{i,1} - \sum_{i\in\mathcal{I}_p^{s_n}}P_{i,1}\Big] \\ & +h_{n,2}h_{p,2}P_{n,2}\Big[\sum_{i\in\mathcal{I}_n^{s_n}}P_{i,2} - \sum_{i\in\mathcal{I}_p^{s_n}}P_{i,2}\Big] \\ & +\sigma^2\big[P_{n,1}(h_{p,1}-h_{n,1}) + P_{n,2}(h_{p,2}-h_{n,2})\big] \\ & \left.\begin{aligned} & +h_{p,1}h_{n,2}\Big[P_{n,1}\sum_{i\in\mathcal{I}_n^{s_n}}P_{i,2} - P_{n,2}\sum_{i\in\mathcal{I}_p^{s_n}}P_{i,1}\Big] \\ & +h_{p,2}h_{n,1}\Big[P_{n,2}\sum_{i\in\mathcal{I}_n^{s_n}}P_{i,1} - P_{n,1}\sum_{i\in\mathcal{I}_p^{s_n}}P_{i,2}\Big]. \end{aligned}\right\} B \end{aligned}$$

By detailing B, we get:

$$\begin{aligned} B = {} & h_{p,1}h_{n,2}\Big[P_{n,1}\Big(\sum_{i\in\mathcal{C}_{pn}^{s_n}}P_{i,2} + \sum_{i\in\mathcal{U}_n}P_{i,2}\Big) \\ & -P_{n,2}\Big(\sum_{i\in\mathcal{C}_{pn}^{s_n}}P_{i,1} + \sum_{i\in\mathcal{U}_p}P_{i,1}\Big)\Big] \\ & +h_{p,2}h_{n,1}\Big[P_{n,2}\Big(\sum_{i\in\mathcal{C}_{pn}^{s_n}}P_{i,1} + \sum_{i\in\mathcal{U}_n}P_{i,1}\Big) \\ & -P_{n,1}\Big(\sum_{i\in\mathcal{C}_{pn}^{s_n}}P_{i,2} + \sum_{i\in\mathcal{U}_n}P_{i,2}\Big)\Big], \end{aligned}$$

$$\begin{aligned} B = {} & (h_{p,1}h_{n,2} - h_{p,2}h_{n,1})\Big[P_{n,1}\sum_{i\in\mathcal{C}_{pn}^{s_n}}P_{i,2} - P_{n,2}\sum_{i\in\mathcal{C}_{pn}^{s_n}}P_{i,1}\Big] \\ & +h_{p,1}h_{n,2}\Big[P_{n,1}\sum_{i\in\mathcal{U}_n}P_{i,2} - P_{n,2}\sum_{i\in\mathcal{U}_p}P_{i,1}\Big] \\ & +h_{p,2}h_{n,1}\Big[P_{n,2}\sum_{i\in\mathcal{U}_n}P_{i,1} - P_{n,1}\sum_{i\in\mathcal{U}_p}P_{i,2}\Big]. \end{aligned}$$

In practical interference-limited systems, the background noise is negligible compared to the interfering signals [36], [37], i.e. $\sigma^2 \ll P_{k',r}h_{k,r}$, $\forall(k,k') \in \mathcal{K}^2, \forall r \in \{1,2\}$. Replacing B by its expression in A, we get the final expression of the SIC condition for the decoding of s_n at the level of user p:

$$\begin{aligned} A = {} & (h_{p,1}h_{n,2} - h_{p,2}h_{n,1})\Big[P_{n,1}\sum_{i\in\mathcal{C}_{pn}^{s_n}}P_{i,2} - P_{n,2}\sum_{i\in\mathcal{C}_{pn}^{s_n}}P_{i,1}\Big] \\ & +h_{n,2}h_{p,2}P_{n,2}\Big[\sum_{i\in\mathcal{U}_n}P_{i,2} - \sum_{i\in\mathcal{U}_p}P_{i,2}\Big] \\ & +h_{p,1}h_{n,2}\Big[P_{n,1}\sum_{i\in\mathcal{U}_n}P_{i,2} - P_{n,2}\sum_{i\in\mathcal{U}_p}P_{i,1}\Big] \\ & +h_{p,2}h_{n,1}\Big[P_{n,2}\sum_{i\in\mathcal{U}_n}P_{i,1} - P_{n,1}\sum_{i\in\mathcal{U}_p}P_{i,2}\Big] \\ & +h_{n,1}h_{p,1}P_{n,1}\Big[\sum_{i\in\mathcal{U}_n}P_{i,1} - \sum_{i\in\mathcal{U}_p}P_{i,1}\Big] > 0. \end{aligned}$$

REFERENCES

[1] M. Mozaffari, W. Saad, M. Bennis, and M. Debbah, "Unmanned aerial vehicle with underlaid device-to-device communications: Performance and tradeoffs," *IEEE Trans. Wireless Commun.*, vol. 15, no. 6, pp. 3949–3963, Jun. 2016.

[2] R. I. Bor-Yaliniz, A. El-Keyi, and H. Yanikomeroglu, "Efficient 3-D placement of an aerial base station in next generation cellular networks," in *Proc. IEEE Int. Conf. Commun. (ICC)*, May 2016, pp. 1–5.

[3] M. Mozaffari, W. Saad, M. Bennis, and M. Debbah, "Drone small cells in the clouds: Design, deployment and performance analysis," in *Proc. IEEE Global Commun. Conf. (GLOBECOM)*, Dec. 2014, pp. 1–6.

[4] M. Alzenad, A. El-Keyi, F. Lagum, and H. Yanikomeroglu, "3-D placement of an unmanned aerial vehicle base station (UAV-BS) for energy-efficient maximal coverage," *IEEE Wireless Commun. Lett.*, vol. 6, no. 4, pp. 434–437, Aug. 2017.

[5] E. Kalantari, H. Yanikomeroglu, and A. Yongacoglu, "On the number and 3D placement of drone base stations in wireless cellular networks," in *Proc. IEEE 84th Veh. Technol. Conf. (VTC-Fall)*, Sep. 2016, pp. 1–6.

[6] B. Li, Z. Fei, and Y. Zhang, "UAV communications for 5G and beyond: Recent advances and future trends," *IEEE Internet Things J.*, vol. 6, no. 2, pp. 2241–2263, Apr. 2019.

[7] Z. Ding, F. Adachi, and H. V. Poor, "Performance of MIMO-NOMA downlink transmissions," in *Proc. IEEE Global Commun. Conf. (GLOBECOM)*, Dec. 2015, pp. 1–6.

[8] Y. Saito, A. Benjebbour, Y. Kishiyama, and T. Nakamura, "System-level performance evaluation of downlink non-orthogonal multiple access (NOMA)," in *Proc. IEEE 24th Annu. Int. Symp. Pers., Indoor, Mobile Radio Commun. (PIMRC)*, Sep. 2013, pp. 611–615.

[9] Y. Saito, Y. Kishiyama, A. Benjebbour, T. Nakamura, A. Li, and K. Higuchi, "Non-orthogonal multiple access (NOMA) for cellular future radio access," in *Proc. IEEE 77th Veh. Technol. Conf. (VTC Spring)*, Jun. 2013, pp. 1–5.

[10] M.-R. Hojeij, J. Farah, C. A. Nour, and C. Douillard, "New optimal and suboptimal resource allocation techniques for downlink non-orthogonal multiple access," *Wireless Pers. Commun.*, vol. 87, no. 3, pp. 837–867, Apr. 2016.

[11] L. Dai, B. Wang, Y. Yuan, S. Han, I. Chih-lin, and Z. Wang, "Non-orthogonal multiple access for 5G: Solutions, challenges, opportunities, and future research trends," *IEEE Commun. Mag.*, vol. 53, no. 9, pp. 74–81, Sep. 2015.

[12] J. Farah, E. Sfeir, C. A. Nour, and C. Douillard, "New resource allocation techniques for base station power reduction in orthogonal and non-orthogonal multiplexing systems," in *Proc. IEEE Int. Conf. Commun. Workshops (ICC Workshops)*, May 2017, pp. 618–624.

[13] M.-J. Youssef, J. Farah, C. A. Nour, and C. Douillard, "Resource allocation in NOMA systems for centralized and distributed antennas with mixed traffic using matching theory," *IEEE Trans. Commun.*, vol. 68, no. 1, pp. 414–428, Jan. 2020.

[14] A. Kilzi, J. Farah, C. A. Nour, and C. Douillard, "New power minimization techniques in hybrid distributed antenna systems with orthogonal and non-orthogonal multiple access," *IEEE Trans. Green Commun. Netw.*, vol. 3, no. 3, pp. 679–690, Sep. 2019.

[15] A. A. Nasir, H. D. Tuan, T. Q. Duong, and H. V. Poor, "UAV-enabled communication using NOMA," *IEEE Trans. Commun.*, vol. 67, no. 7, pp. 5126–5138, Jul. 2019.

[16] M. T. Nguyen and L. B. Le, "NOMA user pairing and UAV placement in UAV-based wireless networks," in *Proc. IEEE Int. Conf. Commun. (ICC)*, May 2019, pp. 1–6.

[17] N. Zhao, X. Pang, Z. Li, Y. Chen, F. Li, Z. Ding, and M.-S. Alouini, "Joint trajectory and precoding optimization for UAV-assisted NOMA networks," *IEEE Trans. Commun.*, vol. 67, no. 5, pp. 3723–3735, May 2019.

[18] X. Mu, Y. Liu, L. Guo, and J. Lin, "Non-orthogonal multiple access for air-to-ground communication," *IEEE Trans. Commun.*, vol. 68, no. 5, pp. 2934–2949, May 2020.

[19] G. Geraci, A. Garcia-Rodriguez, L. Galati Giordano, D. Lopez-Perez, and E. Bjornson, "Understanding UAV cellular communications: From existing networks to massive MIMO," *IEEE Access*, vol. 6, pp. 67853–67865, 2018.

[20] M. D. Michelle and J. S. Harrison. (Aug. 2014). *CoMP (1): CoMP Types-CS, CB, JT and DPS*. [Online]. Available: https://www.netmanias.com/en/post/blog/6558/comp-lte-lte-a/comp- 1-comp-types-cs-cb-jt-and-dps

[21] E. Pateromichelakis, M. Shariat, A. U. Quddus, and R. Tafazolli, "On the evolution of multi-cell scheduling in 3GPP LTE/LTE—A," *IEEE Commun. Surveys Tuts.*, vol. 15, no. 2, pp. 701–717, 2nd Quart., 2013.

[22] A. Kilzi, J. Farah, C. Abdel Nour, and C. Douillard, "Mutual successive interference cancellation strategies in NOMA for enhancing the spectral efficiency of CoMP systems," *IEEE Trans. Commun.*, vol. 68, no. 2, pp. 1213–1226, Feb. 2020.

[23] M.-J. Youssef, C. A. Nour, J. Farah, and C. Douillard, "Backhaul-constrained resource allocation and 3D placement for UAV-enabled networks," in *Proc. IEEE 90th Veh. Technol. Conf. (VTC-Fall)*, Sep. 2019, pp. 1–7.

[24] J. Qin, Z. Wei, C. Qiu, and Z. Feng, "Edge-prior placement algorithm for UAV-mounted base stations," in *Proc. IEEE Wireless Commun. Netw. Conf. (WCNC)*, Apr. 2019, pp. 1–6.

[25] A. Al-Hourani, S. Kandeepan, and A. Jamalipour, "Modeling air-to-ground path loss for low altitude platforms in urban environments," in *Proc. IEEE Global Commun. Conf.*, Dec. 2014, pp. 2898–2904.

[26] A. Al-Hourani, S. Kandeepan, and S. Lardner, "Optimal LAP altitude for maximum coverage," *IEEE Wireless Commun. Lett.*, vol. 3, no. 6, pp. 569–572, Dec. 2014.

[27] D. Tse and P. Viswanath, *Fundamentals of Wireless Communication*. Cambridge, U.K.: Cambridge Univ. Press, 2005, ch. 6, pp. 228–289.

[28] J. Zhu, J. Wang, Y. Huang, S. He, X. You, and L. Yang, "On optimal power allocation for downlink non-orthogonal multiple access systems," *IEEE J. Sel. Areas Commun.*, vol. 35, no. 12, pp. 2744–2757, Dec. 2017.

[29] M. Shipon Ali, H. Tabassum, and E. Hossain, "Dynamic user clustering and power allocation for uplink and downlink non-orthogonal multiple access (NOMA) systems," *IEEE Access*, vol. 4, pp. 6325–6343, 2016.

[30] L. Jaulin and E. Walter, "Set inversion via interval analysis for nonlinear bounded-error estimation," *Automatica*, vol. 29, no. 4, pp. 1053–1064, Jul. 1993.

[31] P. M. Vaidya, "Speeding-up linear programming using fast matrix multiplication," in *Proc. 30th Annu. Symp. Found. Comput. Sci.*, 1989, pp. 332–337.

[32] W. Shi, J. Li, W. Xu, H. Zhou, N. Zhang, S. Zhang, and X. Shen, "Multiple drone-cell deployment analyses and optimization in drone assisted radio access networks," *IEEE Access*, vol. 6, pp. 12518–12529, 2018.

[33] J. Farah, A. Kilzi, C. A. Nour, and C. Douillard, "Power minimization in distributed antenna systems using non-orthogonal multiple access and mutual successive interference cancellation," *IEEE Trans. Veh. Technol.*, vol. 67, no. 12, pp. 11873–11885, Dec. 2018.

[34] J. Choi, "Non-orthogonal multiple access in downlink coordinated two-point systems," *IEEE Commun. Lett.*, vol. 18, no. 2, pp. 313–316, Feb. 2014.

[35] R. Jain, D. Chiu, and W. Hawe, "A quantitative measure of fairness and discrimination for resource allocation in shared computer systems," Eastern Res. Lab., Digit. Equip. Corp., Hudson, MA, USA, DEC Tech. Rep. 301, Sep. 1984.

[36] A. Ghosh, N. Mangalvedhe, R. Ratasuk, B. Mondal, M. Cudak, E. Visotsky, T. A. Thomas, J. G. Andrews, P. Xia, H. S. Jo, H. S. Dhillon, and T. D. Novlan, "Heterogeneous cellular networks: From theory to practice," *IEEE Commun. Mag.*, vol. 50, no. 6, pp. 54–64, Jun. 2012.

[37] H. Tabassum, E. Hossain, and J. Hossain, "Modeling and analysis of uplink non-orthogonal multiple access in large-scale cellular networks using Poisson cluster processes," *IEEE Trans. Commun.*, vol. 65, no. 8, pp. 3555–3570, Aug. 2017.

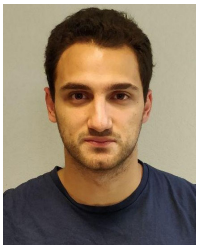

ANTOINE KILZI (Student Member, IEEE) received the computer and communications engineering degree from Lebanese University, in 2017. He is currently pursuing the Ph.D. degree in information and communication engineering with IMT Atlantique. His current research interests include resource allocation, non-orthogonal multiple access, and coordinated multipoint systems.

JOUMANA FARAH (Member, IEEE) received the B.E. degree in electrical engineering from Lebanese University, in 1998, the M.E. degree in signal, image, and speech processing, and the Ph.D. degree in mobile communication systems from the University of Grenoble, France, in 1999 and 2002, respectively, and the Habilitation to Direct Research (HDR) degree from University Pierre and Marie Curie (Paris VI), France. She is currently a full-time Professor with the Faculty of Engineering, Lebanese University, Lebanon. She has supervised a large number of master, Ph.D. theses, and post-docs. She received several research grants from the Lebanese National Council for Scientific Research, the Franco-Lebanese CEDRE program, and Lebanese University. She has nine registered patents and software and has coauthored a research book and more than 100 articles in international journals and conferences. Her current research interests include resource allocation techniques, channel coding, channel estimation, and interference management techniques. She also serves as a TPC member and a reviewer for several journals and conferences. She was the General Chair of the 19th International Conference on Telecommunications (ICT 2012).

CHARBEL ABDEL NOUR (Senior Member, IEEE) received the computer and communications engineering degree from Lebanese University, in 2002, the master's degree in digital communications from the University of Valenciennes, France, in 2003, and the Ph.D. degree in digital communications from Telecom Bretagne, France, in 2008. From June 2007 till October 2011, he worked as a Postdoctoral Fellow with the Department of Electronics, Telecom Bretagne. He was involved in several research projects related to broadcasting and satellite communications. Additionally during the same period, he was active in the Digital Video Broadcasting DVB consortium, where he had important contributions. Starting November 2011, he holds an Associate Professor position at the Department of Electronics, Telecom Bretagne. His research interests include radio mobile communications systems, broadcasting systems, coded modulations, error correcting codes, resource and power allocation for NOMA, waveform design, MIMO, and iterative receivers. Lately, he presented several contributions to the H2020 METIS and FANTASTIC5G projects and to the 3GPP consortium related to coding solutions for 5G.

CATHERINE DOUILLARD (Senior Member, IEEE) received the engineering degree in telecommunications from the Ecole Nationale Supérieure des Télécommunications de Bretagne, France, in 1988, the Ph.D. degree in electrical engineering from the University of Western Brittany, Brest, France, in 1992, and the accreditation to supervise research from the University of Southern Brittany, Lorient, France, in 2004. She is currently a Full Professor with the Department of Electronics, Telecom Bretagne, where she is in charge of the Algorithm-Silicon Interaction research team. Her research interests include turbo codes and iterative decoding, iterative detection, the efficient combination of high spectral efficiency modulation and turbo coding schemes, diversity techniques and turbo processing for multi-carrier, multi-antenna, and multiple access transmission systems. In 2009, she received the SEE/IEEE Glavieux Award for her contribution to standards and related industrial impact. She was active in the Digital Video Broadcasting (DVB) Technical Modules for the definition of DVB-T2 and DVB-NGH as the Chairperson of the Coding, Constellations, and Interleaving task force and DVB-RCS NG standards. Since 2015, she has had several contributions in the FANTASTIC-5G and EPIC H2020 European projects intended for the definition of new techniques for 5G and beyond.